UC San Diego
UC San Diego Previously Published Works

Title

Iminodiacetic Acid as a Novel Metal-Binding Pharmacophore for New Delhi Metallo-β-lactamase Inhibitor Development

Permalink

Journal

ChemMedChem, 15(14)

ISSN

1860-7179

Authors

Chen, Allie Y
Thomas, Caitlyn A
Thomas, Pei W
et al.

Publication Date

2020-07-20

DOI

10.1002/cmdc.202000123

Peer reviewed

Iminodiacetic Acid as a Novel Metal-binding Pharmacophore for New Delhi Metallo-β-lactamase Inhibitor Development

Allie Y. Chen[a], **Caitlyn Thomas**[b], **Pei W. Thomas**[c], **Kundi Yang**[b], **Zishuo Cheng**[b], **Walter Fast**[c], **Michael W. Crowder**[b], **Seth M. Cohen**[a]

[a]Allie Y. Chen, Prof. Seth M. Cohen, Department of Chemistry and Biochemistry, University of California, San Diego, La Jolla, CA 92093, United States

[b]Caitlyn Thomas, Kundi Yang, Prof. Michael W. Crowder, Department of Chemistry and Biochemistry, Miami University, Oxford, OH 45056, United States

[c]Dr. Pei W. Thomas, Prof. Walter Fast, Division of Chemical Biology & Medicinal Chemistry, College of Pharmacy, University of Texas, Austin, Austin, TX 78712, United States

Abstract

The fungal natural product Aspergillomarasmine A (AMA) has been identified as a non-competitive inhibitor of New Delhi Metallo-β-lactamase-1 (NDM-1) that inhibits via active site Zn(II) removal. The non-selective metal-chelating properties and the difficult synthesis and derivatization of AMA have hindered the development of this scaffold into a potent and selective inhibitor of NDM-1. Iminodiacetic acid (**IDA**) has been identified as the metal-binding pharmacophore (MBP) core of AMA that can be leveraged for inhibitor development. Herein, we report the utilization of **IDA** for the fragment-based drug discovery (FBDD) of NDM-1 inhibitors. **IDA** (IC_{50} = 122 μM) was developed into inhibitor **23f** (IC_{50} = 8.6 μM, K_i, = 2.6 μM) and displayed the formation of a ternary complex with NDM-1, as evidenced by protein thermal shift and native state electrospray ionization mass spectrometry (ESI-MS) experiments. Combining mechanistic analysis in tandem with inhibitor derivatization, the utilization of **IDA** as an alternative AMA scaffold for NDM-1 inhibitor development is detailed.

Graphical Abstract

New Delhi Metallo-β-lactamase
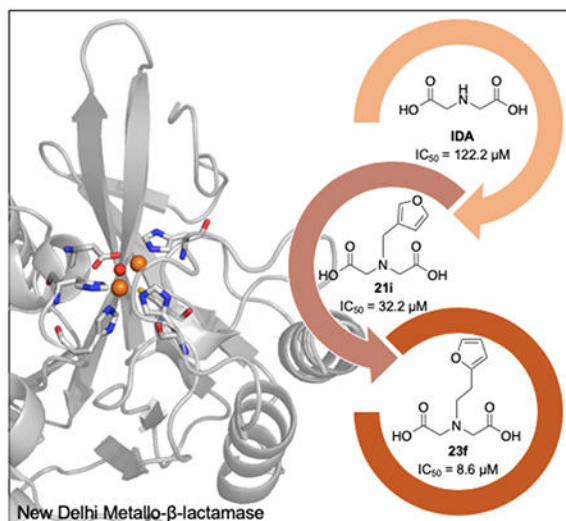
Iminodiacetic acid (IDA) was identified as a novel lead fragment for New Delhi Metallo-β-lactamase (NDM) inhibitor development. Through a series of fragment-based drug design, synthesis, and mechanistic analysis, **23f** was identified as a potent inhibitor. This inhibitor represents the potential to convert traditional metal chelators to one that displays the formation of a ternary complex. The IDA fragment and inhibitors reported provide a roadmap for future metallô-lactamase inhibitor development.

Keywords

Metal-binding Pharmacophore (MBP); Aspergillomarasmine A (AMA); Iminodiacetic Acid (IDA); Metal Chelator; New Delhi Metallo-β-lactamase (NDM); antibiotic resistance

Introduction

A recent report published by the Centers for Disease Control and Prevention (CDC) estimated that antibiotic-resistant bacteria and fungi cause >2.8 million cases of infections in the United States each year, with >35,000 of those cases resulting in death.[1] Resistance mechanisms (including mutation of penicillinbinding proteins, production of efflux pumps, and expression of β-lactamases) evolved and employed by pathogens are a prime example of bacterial adaptability and pose an urgent threat to the public health.[2] The most valuable class of drugs for combating bacterial infections include β-lactam antibiotics. This class of antibiotics acts as a substrate analogue to obstruct peptidoglycan chain cross-linking in bacterial cell wall biosynthesis and accounts for ~65% of all injectable antibiotics prescribed in the United States.[3] However, the over-use of β-lactams has led to the evolution of β-lactamases, enzymes that hydrolyze the β-lactam ring to render the drug ineffective. Three classes of β-lactamases, Ambler class A, C, and (serin-β-lactamases, SBLs) utilize an active site serine residue for hydrolysis, while one class of β-lactamase, Ambler class B (metallo-β-lactamase, MBL) utilizes a metal center to initiate ring cleavage.[2a, 4] Merely two decades after the introduction of penicillin in the 1940s, the first observed MBL was reported.[5] Currently, there are >80 unique MBL families.[3] With their wide substrate profile (able to

hydrolyze virtually all clinically used bicyclic p-lactam antibiotics), MBLs have risen to become one of the most problematic resistance mechanisms.[6] Detailed reviews on MBLs can be found elsewhere.[7]

Depending on protein sequence homology and number of Zn(II) ions in the catalytic site, MBLs are divided into three subclasses (B1, B2, and B3). The most prevalent members belong to subclass B1 and include IMiPenemase (IMP), Verona Integron-encoded Metallo-β-lactamase (VIM), and New Delhi Metallo-β-lactamase (NDM).[6, 8] NDM is the most recent member of the trio, with its genetic and biochemical characterization first reported in 2009 upon isolation from carbapenem-resistant *Klebsiella pneumoniae*.[9] The rapid spread of NDM is attributed to many factors, including the ability for *bla*NDM-gene bearing plasmids to undergo horizontal gene transfer between different species of microorganisms and to co-harbor genes that encode for other resistance factors.[9–10] In contrast to other MBLs (which are soluble periplasmic proteins), NDM is a lipoprotein that anchors to bacterial outer membrane and displays increased protein stability and secretion.[11] Additionally, NDM variants (>24 reported to date) have evolved to overcome metal scarcity and increased thermal stability.[11c, 12] The NDM active site bears two Zn(II) ions, with Zn_1 ligated by H116, H118, H196, and a bridging hydroxide in a tetrahedral coordination geometry, and Zn_2 ligated by D120, C221, H263, the bridging hydroxide, and an apical H_2O in a trigonal bipyramidal coordination geometry (standard BBL numbering, Figure 1).[13] The binding pocket of NDM has a volume of 591 $Å^3$, which is nearly 2-fold larger in comparison to that of IMP (303 $Å^3$) and almost 4-fold larger compared to that of VIM (140 $Å^3$).[14] This highly plastic and large cavity accommodates a wide range of antibiotic substrates and allows for the efficient hydrolysis of nearly all β-lactam antibiotics.[15]

There are currently >500 distinct NDM inhibitors reported in literature (representative structures show in Figure 2).[16] An important class of compounds bear a sulfhydryl-motif (including D/L-captopril and bisthiazolidines) that act via a competitive inhibition mechanism by displacing the bridging hydroxide ion to form a μ-bridging species between the Zn(II) ions.[17] Another important class of inhibitors includes the cyclic boronates, which have been shown to successfully pan-inhibit SBLs and MBLs via a tetrahedral anionic transition state mimetic.[18] Notably, taniborbactam (VNRX-5133) is the only candidate to have advanced to the clinic (currently in phase III clinical trials).[18c]

The last class includes compounds that bear metal-chelating motifs.[19] Of these, the fungal natural product Aspergillomarasmine A (AMA, IC_{50} = 4 – 7 μM, Figure 2), an aminopolycarboxylic acid, has gained attention due to its ability to restore meropenem activity in a mouse infected with NDM-1 expressing *Klebsiella pneumoniae*.[19e, 20] AMA inhibitor development has focused on modification of the carboxylic acid functional groups through removal or conversion to an ester motif, or exploration of related aminocarboxylic acid analogues.[20b, 21] AMA-1 and AMA-2 (Figure 2), where one of the carboxylate groups is replaced with a methyl substituent yielded weaker inhibition (IC_{50} = 22 and 94 μM, respectively) compared to that of AMA, validating the requirement of free carboxylic acids for enzyme inactivation and supporting the mechanism of action of AMA is via non-selective Zn(II) sequestration (similar to that of EDTA). The metal-chelating properties of AMA along with difficult synthesis and derivatization routes has hindered the development

of this motif into NDM-1 inhibitors.[21a, 22] Structural comparison of AMA and EDTA reveals iminodiacetic acid (**IDA**) as a privileged scaffold that could be leveraged for NDM-1 inhibitor development (Figure 2, highlighted in bold). **IDA** is a strong tridentate metal chelator (via its *O,N,O*-donor atoms), as evidenced by its role in immobilized metal affinity chromatography (IMAC)[23] and its development for the sequestration of Zn(II) in IDA-modified human lysozyme (IDA-hLys) against Zn(II)-mediated Aβ-aggregation for the treatment of Alzheimer's disease.[24] Utilization of **IDA** for inhibitor development allows for greater synthetic accessibility of derivatives to probe the NDM-1 active site and to develop inhibitors that form stable ternary complexes. In addition, **IDA** bears structural resemblance to the hydrolyzed antibiotic β-lactam ring, suggesting the potential for the development of transition-state analogue inhibitors. Notably, **IDA** is an aliphatic derivative of the previously investigated dipicolinic acid inhibitor,[19d] further justifying its use as a scaffold for novel NDM-1 inhibitor development (Figure 2, highlighted in bold).

Herein, we report the utilization of **IDA** as a novel metal-binding pharmacophore (MBP) for NDM-1 inhibitor development. Through fragment-based drug discovery (FBDD), the **IDA** MBP ($IC_{50} = 122$ μM) was developed into the lead inhibitor **23f** ($IC_{50} = 8.6$ μM) against NDM-1. Protein thermal shift and native state electrospray ionization mass spectrometry (ESI-MS) experiments revealed **23f**, and related derivatives, inhibits NDM-1 via the formation of a stable NDM-1:Zn(II):**23f** ternary complex. This work demonstrates the potential in the **IDA** scaffold for NDM-1 inhibitor development and provides a roadmap for future **IDA** derived inhibitors.

Results and Discussion

IDA MBP Design and Synthesis.

To verify **IDA** as a potential MBP lead for inhibitor design, a small library of MBP compounds bearing structural similarity to **IDA** was assembled and their inhibitory activity against NDM-1 was assessed (Table 1). This library included compounds that have at least one nitrogen atom and one carboxylate functional group for bidentate metal-binding (*N,O*-donor atoms). The *N*-donor atom in the MBPs were either a tertiary amine (**1**), secondary amine (**IDA, 2 – 4**), or aromatic amine (**5 – 10**). These MBPs were screened at a single concentration of 200 μM via an enzymatic assay which monitored the NDM-1 mediated hydrolysis of the substrate meropenem.[25] Evaluation of this library revealed **IDA** to be the only MBP with a secondary amine *N*-donor atom to yield significant inhibition activity (48%). MBPs **2 – 4**, where the secondary amine is a part of the saturated ring, did not display any appreciable inhibition (8%). A methylated **IDA** derivative (**1**), was the most potent of this library, reaching 80% inhibition. Some MBPs bearing the aromatic amine motif showed some inhibitory activity, with **8** displaying the second highest inhibition value (57%). Data from this small set of MBPs suggest a preference for a tertiary or aromatic heterocycle *N*-donor atom. These findings verified the **IDA** MBP as a viable scaffold for NDM-1 inhibitor development. Based on these findings, MBP **1** was chosen for further investigation.

A second-generation of **IDA** derivatives (Table 2) were synthesized according to Scheme 1 – Scheme 3. Compounds in this sublibrary incorporated a benzyl substituent, as aromatic rings have previously been shown to form favorable hydrophobic interactions with the NDM β-hairpin loop.[16] Utilizing the concept of bioisosteric replacement, **IDA** derivatives where one carboxylic acid was modified (**13a**, **13b**, **15**, **17**) were prepared to determine if both carboxylic acids were necessary for inhibition and if alternative MBPs could achieve increase potency. Compounds where the methyl- or benzyl-substituent (**19a** – **19d**) was placed at the α-carbon were explored as well. The compounds were screened against at a single concentration of 250 μM against NDM-1. The methylated-IDA (**1**) remained the most potent of the series, exhibiting 90% inhibition at 250 μm. The benzylated-**IDA** (**11**) was the second most potent (65%). Interestingly, bioisosteres with a propionic acid motif (**13a** and **13b**, which are most structurally similar to AMA) displayed a complete loss of activity. While the phosphate isostere (**15**) showed no inhibition against NDM-1, the less acidic tetrazole isostere (**17**) showed inhibition that was comparable to that of **11**. Notably, there was no preference for *R*- or *S*- stereoisomers at the α-carbon position of **IDA**, as evident by similar inhibitory values (51 – 65%) displayed by derivatives **19a** – **19d**.

IDA Derivative Synthesis and Inhibitory Activity.

Compounds **1** and **11** were selected as scaffolds for inhibitor development, and additional **IDA** derivatives with various substituents were prepared. This sublibrary was prepared using a double substitution reaction of various primary amines with *t*-butyl 2-bromoacetate to yield compounds **21a** – **21m** (Scheme 4, Table 3). The sublibrary was screened at a single inhibitor concentration of 250 μM. The majority of the compounds in this sublibrary inhibited NDM-1 at an appreciable level (~60%); however, no clear SAR could be elucidated. Compared to the percent inhibition of **11** (65%, Table 2), modification via an ethyl-linker (**21a**) or a bi-phenyl substituent (**21b** and **21c**) did not result in substantial inhibition improvements (56 – 76%). Notably, compounds bearing a phenyl- or benzyl-sulfonamide motif (**21j** and **21k**) displayed a complete loss of activity (most likely due to the reduced basicity of the central nitrogen); however, substitution with a thiophene substituent (**21l** and **21m**) restored activity by ~20%. In addition, **21i** stood out as the most potent inhibitor of this sublibrary with almost complete inhibition against NDM-1 (~99%). When the heterocyclic oxygen is swapped out for a sulfur (**21h**), the inhibition activity is reduced to 64%, showing a preference for the furan substituent.

To further develop inhibitors against NDM-1 and investigate the difference in inhibitory activity between the furan and thiophene substituents, a second library bearing analogues of **21h** and **21i** were synthesized and evaluated (**23a** – **23h**, Table 4). In general, all derivatives bearing a furan motif exhibited a lower IC_{50} value compared to that of the corresponding thiophene derivative. These results validate a preference for an oxygen heteroatom. While the 1,2-furan (**23b**, IC_{50} = 22 μM) displayed a lowered IC_{50} value compared to that of the 1,3-furan (**21i**, IC_{50} = 32 μM), the introduction of a methyl substituent at the 5-positon (**23d**, IC_{50} = 47 μM) resulted in poorer activity. Extension from a methyl-linker (**23b**) to an ethyl-linker (**23f**) resulted in a 2.5-fold fold improvement in inhibitory activity and resulted in the most potent inhibitor of this sublibrary (IC_{50} = 8.6 μM). It is predicted that the ethyl linker allows for the furan substituent to make more favorable interactions with the base of the L3

β-hairpin loop of NDM-1, as observed in the crystal structure of hydrolyzed antibiotic cefuroxime complexed with NDM-1 (PDB 5O2E);[24] however, further experiments are required to confirm the specific ligand-protein interactions. The corresponding thiophene derivatives displayed the same trends, albeit with poorer inhibition values. Due to the strong affinity **IDA** has for Zn(II) ions ($K_d = 3.2 \times 10^{-5}$ M)[26] and the analysis of inhibition mechanism (vide infra), we propose that **23f** binds via coordination to the Zn(II) ions at the NDM-1 protein active site via a competitive mechanism of action. The Cheng-Prusoff relationship[27] for competitive inhibitors enables calculation of K_i of 2.6±0.3 μM for **23f**. Two methods, thermal shift and native state ESI-MS, were utilized to interrogated the mode of inhibition of selected inhibitors. Compared to alternative methods (such as NMR, crystallography, equilibrium dialysis, and others), thermal shift assay and native state ESI-MS utilize relatively lower protein and inhibitor concentrations, and are more amenable to high-throughput analysis, making them a suitable approach for initial mechanistic studies.

Protein Thermal Shift Assay.

Protein thermal shift assay detects ligand-induced protein stabilization, and has emerged as a valuable tool for hit-identification and validation methodology in drug discovery.[28] Herein, we utilize this general method to validate **IDA** derivatives as inhibitors of NDM-1 and evaluate their propensity to remove Zn(II) from the active site of NDM-1. In this assay, a fluorescent dye is utilized to monitor the difference in the unfolding temperature of the native protein versus the inhibitor-bound protein. The inhibitor-bound protein generally has greater protein stability and increases the melting temperature (positive T_m, as observed with L-captopril, Table 5).[29] In contrast, the removal of Zn(II) has been observed to destabilize the protein and results in a negative T_m (as seen with **DPA**).[12b] It is important to note that while reported thermal shift data have revealed a good correlation between the observed IC_{50} value and T_m,[30] this correlation has not been observed for inhibitors of NDM-1.[29, 31] In the case of the compounds tested here, T_m did not correlate with IC_{50} values. All tested compounds displayed a range of positive T_m values, with **IDA**, **21h**, **23c**, and **23h** yielding T_m on par with, or better than, that of L-captopril. Although no correlation was observed, the small, positive T_m shifts exhibited by all derivatives represents the absence of Zn(II)-chelation and is suggestive evidence for the formation of ternary complexes.

Native State Electrospray Ionization Mass Spectrometry.

Native state ESI-MS was used to further investigate the formation of an NDM-1 :Zn(II):inhibitor ternary complex of derivatives **1** and **23c** – **23f** against NDM-1 and VIM-2. This method allows for the rapid determination of the changes in NDM-1:Zn(II):inhibitor stoichiometry.[32]. The major advantage of ESI-MS is in its ability to analyze for the formation of a ternary complex using near physiological concentrations of enzyme and inhibitor. Briefly, NDM-1 and VIM-2 (at 10 μM) were incubated for approximately 5 min with each inhibitor (50 μM) prior to analysis. The control spectra of native NDM-1 revealed a dominant +9 peak at 2,822 *m/z*, corresponding to the mass of di-Zn(II) NDM-1 (25,385 Da, Table 6, Figure S1). In contrast, incubation of NDM-1 with **DPA**, a metal chelator, resulted in +9 peaks at 2,807 *m/z*, 2,814 *m/z*, and 2,822 *m/z*, corresponding to the presence of apo-, mono-Zn(II) and di-Zn(II) NDM-1, respectively.

These results were similar to the observed spectra of NDM-1 with EDTA, which showed a dominant peak corresponding to metal free NDM-1 (unpublished data). It is important to note that the current native ESI-MS experiment procedures do not generate quantitative results. Higher relative peak intensities (dominant peaks) do not indicate higher concentrations of the solution species, but rather the species that is best ionized by the mass analyzer.[33]

The spectra of NDM-1 incubated with inhibitors **1** and **23c** – **23f** all showed the presence of ternary complexes, with the predicted and observed peaks summarized in Table 6 (Figure S1). In all of these experiments, in addition to the dominant di-Zn(II) NDM-1 peak, an additional peak corresponding to the mass of di-Zn(II) NDM-1 plus inhibitor was observed. Protein incubation with derivative **1** revealed a less dominant di-Zn(II) NDM-1:**1** +9 peak at 2,837 *m/z* (25,532 Da). Incubation of protein with **23c** yielded +9 and +8 peaks at 2,850 *m/z* and 3,210 *m/z*, respectively, corresponding to the di-Zn(II) NDM-1:**23c** complex (25,628 Da). Similarly, incubation of protein with **23d** yielded +9 and +8 peaks at 2,846 *m/z* and 3,202 *m/z*, corresponding to the di-Zn(II) NDM-1:**23d** complex. Inhibitor **23e** produced a significantly less intense +9 and +8 peaks at 2,847 *m/z* and 3,205 *m/z*, corresponding to the di-Zn(II) NDM-1:**23e** complex (25,628 Da). Lastly, incubation of NDM-1 with lead inhibitor **23f** revealed a less intense +9 peak at 2,848 *m/z* and a more intense +8 peak at 3,202 *m/z*, both of which correspond to the mass of di-Zn(II) NDM-1:**23f** (25,612 Da, Figure 3).

Previous work has shown that different mechanisms of inhibition can be observed for the same inhibitors against varying MBLs (unpublished data). To verify that the **IDA** inhibitors are able to form ternary complexes with other MBLs and have the potential to be developed into pan-MBL inhibitors, additional ESI-MS experiments were performed for inhibitors **1** and **23c** – **23f** with VIM-2. Control spectra of VIM-2 revealed dominant +9 and +8 peaks at 2,886 *m/z* and 3,247 *m/z*, respectively, corresponding to the mass of di-Zn(II) VIM-2 (25,972 Da, Table 7, Figure S2). VIM-2 incubated with **DPA** revealed dominant +9 and +8 peaks at 2,891 *m/z* and 3,253 *m/z*, respectively, corresponding most closely with the mass of apo-VIM-2 with 1 equivalent of **DPA** bound (26,010 Da).

Similar to the previously reported NDM-1:inhibitor complexes, spectra of VIM-2 incubated with inhibitors **1** and **23c** – **23f** all revealed the presence of ternary complexes. In addition to the dominant di-Zn(II) VIM-2 peak, additional di-Zn(II) VIM-2:inhibitor peaks were observed. The predicted and observed peaks are summarized in Table 7 (Figure S2). Incubation of VIM-2 with 1 revealed a less dominant +9 peak at 2,902 *m/z*, corresponding to di-Zn(II) VIM-2:1 complex (26,119 Da). The native MS of VIM-2 incubated with inhibitors **23c** – **23f** displayed similar secondary peaks at 3,277 *m/z* (26,215 Da), 3,276 *m/z* (26,199 Da), 3,277 *m/z* (26,215 Da), and 3,278 *m/z* (26,199 Da) representing the formation of the di-Zn(II) VIM-2:**23c**, di-Zn(II) VIM-2:**23d**, di-Zn(II) VIM-2:**23e**, and di-Zn(II) VIM-2:**23f** (Figure 3) ternary complex, respectively. This data is evident that the representative **IDA** inhibitors form ternary complexes with VIM-2, and represents a promising scaffold for future development against other MBLs.

Conclusion

Since the discovery of AMA as an effective inhibitor against NDM-1 capable of restoring the efficacy of antibiotic meropenem in mouse models, the synthesis and development of this compound into a more potent and selective inhibitor have been of interest.[19e, 22a, 22b] AMA, similar to EDTA, is a non-competitive inhibitor that deactivates NDM-1 via active site Zn(II) metal sequestration.[20a] Inhibitor development of AMA through modification of the carboxylic acid functional groups has been unsuccessful, as that motif is necessary for metal-chelation.[21a] Herein, we report the FBDD of **IDA** as a novel MBP for NDM-1 inhibitor development. **IDA** is a simplified analogue of AMA and EDTA, allowing for more facile inhibitor derivatization to probe the NDM-1 active site pocket. Reducing the number of carboxylates should also reduce the affinity of these compounds for free Zn(II) ions, thereby reducing their metal-stripping propensity. From a preliminary screen of a small library of MBPs, **IDA** and **1** were verified as novel hits for inhibitor development. Upon rounds of library design, synthesis, and mechanistic analysis **IDA** (IC_{50} = 122 μM) was developed into inhibitor **23f** (IC_{50} = 8.6 μM). To study the mode of inhibition, protein thermal shift and native state ESI-MS were utilized. Both experiments revealed **23f** and related derivatives inhibited NDM-1 via the formation of stable ternary complexes. Additional studies are currently underway to elucidate the precise protein-inhibitor binding interactions; however, similarities are observed with optimized dipicolinic acid derivatives.[19d] Each scaffold is optimized through the addition of a central hydrophobic substituent that includes a hydrogen-bond partner that appears to require precise positioning, presumably reflecting the binding interactions made with the beta-hairpin loop neighboring the di-nuclear Zn(II) ion site of NDM-1. While lead compound **23f** displayed an inhibitory value similar to that of AMA (IC_{50} = 4 – 9 μM), rational inhibitor design integrated with detailed mechanistic studies has allowed for the development of an AMA-inspired alternative that displays the formation of a NDM-1:Zn(II):inhibitor ternary complex with a K_i of 2.6 μM. This work represents the benefit of performing mechanistic analysis hand-in-hand with inhibitor derivation for the development of inhibitors with a mode of inhibition more suitable for drug development. By utilizing a novel **IDA** MBP scaffold, traditional metal chelators (such as AMA and EDTA) not viewed as candidates for inhibitor development can be elaborated into potent inhibitors that form favorable ternary complexes. Our findings provide a path for the development of **IDA**-based inhibitors against NDM-1 and other clinically relevant MBLs. Upon the development of advance inhibitors with greater potency and selectivity, detailed spectroscopy and microbiology studies can be performed to further validate the mechanism of action.

Experimental Section

Inhibitors **1** – **11**, **IDA**, reagents, and solvents were obtained from commercial sources and used without further purification. All reactions, unless otherwise stated, were performed at room temperature under a nitrogen atmosphere. Flash column chromatography was performed using a Teledyne ISCO CombiFlash Rf system using hexanes, ethyl acetate, dichloromethane, and methanol as eluents with prepacked silica cartridges. Reverse phase column chromatography was performed on the same instrument using methanol and water (w/ 0.1% formic acid) as eluents with high-performance Gold C18 columns. Column

separation was monitored via Teledyne ISCO RF+ Purlon ESI-MS. ^{1}H and ^{13}C NMR spectra were recorded at ambient temperature on a 400 Varian Mercury Plus or 500 Varian VX NMR instrument located in the Department of Chemistry and Biochemistry at the University of California, San Diego. Mass spectra were obtained at the Molecular Mass Spectrometry Facility (MMSF) in the Department of Chemistry and Biochemistry at the University of California, San Diego. The purity of all compounds used in assays was determined to be ≥95% by high-performance liquid chromatography. Enzymatic assays were performed via monitoring the hydrolysis of substrate meropenem on Synergy H4 Hybrid Microplate Reader using 96-well UV-transparent microplates #3635 (Corning) according to previously published procedures.[25] Thermal shift assays were performed on QuantStudio 3 real-time PCR machines (Applied Biosystems) using 96-well 0.2 mL optical MicroAmp thermocycler plates and SYPRO orange Thermal Shift dye (ThermoFisher). Native state ESI-MS experiments were performed on a LTQ Orbitrap XL hybrid ion trap-orbitrap mass spectrometer (ThermoScientific).

Synthesis

tert-Butyl 3-((2-(*tert*-butoxy)-2-oxoethyl)(methyl)amino)propanoate (12a). Clear colorless oil, yield: 90% (676 mg, 2.47 mmol).

3-((Carboxymethyl)(methyl)amino)propanoic acid (13a). White solid, quantitative yield (102 mg, 0.40 mmol).

tert-Butyl 3-(benzyl(2-(*tert*-butoxy)-2-oxoethyl)amino)propanoate (12b). Clear colorless oil, yield: 43% (239 mg, 0.67 mmol).

3-(Benzyl(carboxymethyl)amino)propanoic acid (13b). White solid, quantitative yield (168 mg, 0.47 mmol).

Ethyl *N*-benzyl-*N*-(2-(diethoxyphosphoryl)ethyl)glycinate (14). Clear colorless oil, yield: 40% (150 mg, 0.42 mmol).

N-Benzyl-*N*-(2-phosphonoethyl)glycine (15). White solid, yield: 99% (114 mg, 0.42 mmol).

Ethyl *N*-benzyl-*N*-(cyanomethyl)glycinate (16). Clear colorless oil, yield: 74% (447 mg, 1.92 mmol).

N-((1*H*-tetrazol-5-yl)methyl)-*N*-benzylglycine (17). Yellow solid, yield: 18% (40.0 mg, 0.16 mmol).

General procedures for the synthesis of 19a – 19d

To a solution of the corresponding amine (1.1 equivalents) and TEA (2 equivalents) in DMF (10 mL) was added *t*-butyl 2-bromoacetate (1 equivalent) dropwise at 0°C. The reaction was allowed to warm to 25 °C and stirred for additional 16 h. After completion of the reaction, the salts were removed via vacuum filtration. The collected filtrate was concentrated in vacuo and the residue was purified via flash column chromatograph to afford the desired intermediates **18a** – **18d**. Intermediates were dissolved in TFA:CH$_2$Cl$_2$ (4:1 mL) and the

reaction mixture was stirred at 25 °C for 16 h. The excess TFA removed via coevaporation with copious amounts of MeOH under reduced pressure. The product was purified via reverse phase column chromatography using MeOH in H_2O (w/ 0.1% formic acid) as eluent to afford the title compounds **19a** – **19d**.

***tert*-Butyl (2-(*tert*-butoxy)-2-oxoethyl)-D-alaninate (18a)**. Clear oil, yield: 40% (175 mg, 0.68 mmol).

(Carboxymethyl)-D-alanine (19a). Clear oil, yield: 99% (93 mg, 0.63 mmol).

***tert*-Butyl (2-(*tert*-butoxy)-2-oxoethyl)-L-alaninate (18b)**. Clear oil, yield: 40% (176 mg, 0.68 mmol).

(Carboxymethyl)-L-alanine (19b). White solid, yield: 99% (72 mg, 0.49 mmol).

***tert*-Butyl (2-(*tert*-butoxy)-2-oxoethyl)-D-phenylalaninate (18c)**. Clear oil, yield: 52% (296 mg, 0.88 mmol).

(Carboxymethyl)-D-phenylalanine (19c). White solid, yield: 98% (116 mg, 0.52 mmol).

***tert*-Butyl (2-(*tert*-butoxy)-2-oxoethyl)-L-phenylalaninate (18d)**. Clear oil, yield: 54% (308 mg, 0.92 mmol).

(Carboxymethyl)-L-phenylalanine (19d). White solid, yield: 98% (110 mg, 0.49 mmol).

General procedures for the synthesis of 21a – 21m and 23a – 23h

The synthesis of compounds **21a** – **21m** and **23a** – **23h** were adapted from literature reported procedures.[34] To a solution of the corresponding amine (1 equivalent) and KHCO3 (4 equivalents) in THF or DMF (10 mL) was added *t*-butyl 2-bromoacetate (2.25 equivalents), and the reaction was stirred at 25 °C for 16 h. After completion of the reaction, as indicated by TLC, the salts were removed via vacuum filtration. The collected filtrate was concentrated in vacuo and the residue was purified via flash column chromatograph using hexane/ethyl acetate as eluent to afford the desired intermediates **20a** – **20m** and **22a** – **22h**. Compounds **21a** – **21m** and **23a** – **23h** were obtained through the following deprotection procedures: A) Intermediate was dissolved in a mixture of TFA:CH_2CI_3 (4:1 mL) and the reaction was stirred at 25 °C for 16 h. The excess TFA was removed under reduced pressure and co-evaporated with copious amounts of MeOH. The acid product was purified via reverse phase column chromatography with MeOH and H2O (w/ 0.1% formic acid) as eluent to afford the desired products; or B) Intermediate was dissolved in 1M NaOH:THF:MeOH (3:1:1 mL) and the reaction mixture was stirred at 65 °C for 16 h. THF and MeOH was removed under reduced pressure and the aqueous solution was acidified to pH 5 with 4M HCl. The precipitate was collected via vacuum filtration.

Di-*tert*-butyl 2,2'-(phenethylazanediyl)diacetate (20a). Viscous clear colorless oil, yield: 84% (708 mg, 2.03 mmol).

2,2'-(Phenethylazanediyl)diacetic acid (21a). Deprotection procedure A. White solid, yield: 99% (104 mg, 0.44 mmol).

Di-*tert*-butyl 2,2'-(([1,1'-biphenyl]-4-ylmethyl)azanediyl)diacetate (20b). White fluffy solid, yield: 69% (680 mg, 1.65 mmol).

2,2'-(([1,1'-Biphenyl]-4-ylmethyl)azanediyl)diacetic acid (21b). Deprotection procedure A. White solid, yield: 99% (72 mg, 0.24 mmol).

Di-*tert*-butyl 2,2'-(([1,1'-biphenyl]-3-ylmethyl)azanediyl)diacetate (20c). Clear colorless oil, yield: 98% (967 mg, 2.35 mmol).

2,2'-(([1,1'-Biphenyl]-3-ylmethyl)azanediyl)diacetic acid (21c). Deprotection procedure A. White solid, yield: 98% (141 mg, 0.47 mmol).

Di-*tert*-butyl 2,2'-((4-hydroxybenzyl)azanediyl)diacetate (20d). White solid, yield: 63% (530 mg, 1.51 mmol).

2,2'-((4-Hydroxybenzyl)azanediyl)diacetic acid (21d). Deprotection procedure A. White solid, yield: 99% (105 mg, 0.44 mmol).

Di-*tert*-butyl 2,2'-((4-chlorobenzyl)azanediyl)diacetate (20e). White crystalline solid, yield: 82% (727 mg, 1.97 mmol).

2,2'-((4-Chlorobenzyl)azanediyl)diacetic acid (21e). Deprotection procedure A. White solid, yield: 98% (120 mg, 0.48 mmol).

Di-*tert*-butyl 2,2'-((4-cyanobenzyl)azanediyl)diacetate (20f). White crystalline solid, yield: 75% (1.30 g, 3.60 mmol).

2,2'-((4-Cyanobenzyl)azanediyl)diacetic acid (21f). White solid, yield: 94% (67 mg, 0.27 mmol).

Di-tert-butyl 2,2'-((4-(1H-tetrazol-5-yl)benzyl)azanediyl)diacetate (20g). Pale yellow solid, yield: 46% (130 mg, 0.32 mmol).

2,2'-((4-(1H-Tetrazol-5-yl)benzyl)azanediyl)diacetic acid (21g). Deprotection procedure B. Beige solid, yield: 54% (50 mg, 0.17 mmol).

Di-*tert*-butyl 2,2'-((thiophen-3-ylmethyl)azanediyl)diacetate (20h). Yellow oil, yield: 62% (506 mg, 1.48 mmol).

2,2'-((Thiophen-3-ylmethyl)azanediyl)diacetic acid (21h). Deprotection procedure A. White solid, yield: 80% (118 mg, 0.52 mmol).

Di-*tert*-butyl 2,2'-((furan-3-ylmethyl)azanediyl)diacetate (20i). Clear colorless oil, yield: 29% (230 mg, 0.71 mmol).

2,2'-((Furan-3-ylmethyl)azanediyl)diacetic acid (21i). Deprotection procedure A. White solid, yield: 99% (179 mg, 0.84 mmol).

Di-*tert*-butyl 2,2'-((phenylsulfonyl)azanediyl)diacetate (20j). White crystalline solid, yield: 70% (273 mg, 0.71 mmol).

2,2'-((Phenylsulfonyl)azanediyl)diacetic acid (21j). Deprotection Procedure A. White solid, yield: 100% (115 mg, 0.42 mmol).

Di-*tert*-butyl 2,2'-((benzylsulfonyl)azanediyl)diacetate (20k). White solid, yield: 76% (310 mg, 0.78 mmol).

2,2'-((Benzylsulfonyl)azanediyl)diacetic acid (21k). Deprotection Procedure A. White solid, yield: 99% (90 mg, 0.31 mmol).

Di-*tert*-butyl 2,2'-((thiophen-2-ylsulfonyl)azanediyl)diacetate (20l). White crystalline solid, yield: 77% (308 mg, 0.79 mmol).

2,2'-((Thiophen-2-ylsulfonyl)azanediyl)diacetic acid (21l). Deprotection Procedure A. Off-white solid, yield: 90% (105 mg, 0.38 mmol).

Di-*tert*-butyl 2,2'-((benzo[b]thiophen-2-ylsulfonyl)azanediyl)diacetate (20m). Off-white crystalline solid, yield: 70% (312 mg, 0.71 mmol).

2,2'-((Benzo[b]thiophen-2-ylsulfonyl)azanediyl)diacetic acid (21m). Deprotection Procedure A. Yellow solid, yield: 99% (101 mg, 0.31 mmol).

Di-*tert*-butyl 2,2'-((thiophen-2-ylmethyl)azanediyl)diacetate (22a). Clear colorless oil, yield: 87% (717 mg, 2.10 mmol).

2,2'-((Thiophen-2-ylmethyl)azanediyl)diacetic acid (23a). Deprotection Procedure A. White solid, yield: 70% (130 mg, 0.57 mmol).

Di-*tert*-butyl 2,2'-((furan-2-ylmethyl)azanediyl)diacetate (22b). Yellow oil, yield: 82% (646 mg, 1.99 mmol).

2,2'-((Furan-2-ylmethyl)azanediyl)diacetic acid (23b). Deprotection Procedure A. Yellow oil, yield: 99% (160 mg, 0.75 mmol).

Di-*tert*-butyl 2,2'-(((5-methylthiophen-2-yl)methyl)azanediyl)diacetate (22c). Clear colorless oil, yield: 82% (700 mg, 1.97 mmol).

2,2'-(((5-Methylthiophen-2-yl)methyl)azanediyl)diacetic acid (23c). Deprotection Procedure A. Yellow solid, yield: 97% (113 mg, 0.46 mmol).

Di-*tert*-butyl 2,2'-(((5-methylfuran-2-yl)methyl)azanediyl)diacetate (22d). Clear colorless oil, yield: 64% (522 mg, 1.54 mmol).

2,2'-(((5-Methylfuran-2-yl)methyl)azanediyl)diacetic acid (23d). Deprotection Procedure B. Yellow solid, yield: 53% (70 mg, 0.31 mmol).

Di-*tert*-butyl 2,2'-((2-(thiophen-2-yl)ethyl)azanediyl)diacetate (22e). Light yellow oil, yield: 85% (726 mg, 2.04 mmol).

2,2'-((2-(Thiophen-2-yl)ethyl)azanediyl)diacetic acid (23e). Deprotection Procedure A. White solid, yield: 75% (109 mg, 0.45 mmol).

Di-*tert*-butyl 2,2'-((2-(furan-2-yl)ethyl)azanediyl)diacetate (22f). Yellow oil, yield: 84% (683 mg, 2.01 mmol).

2,2'-((2-(Furan-2-yl)ethyl)azanediyl)diacetic acid (23f). Deprotection Procedure A. Yellow solid, yield: 33% (24 mg, 0.11 mmol).

Di-*tert*-butyl 2,2'-(((5-bromothiophen-2-yl)methyl)azanediyl)diacetate (22g). Yellow crystalline solid, yield: 90% (908 mg, 2.16 mmol).

2,2'-(((5-Bromothiophen-2-yl)methyl)azanediyl)diacetic acid (23g). Deprotection Procedure A. White crystalline solid, yield: 98% (108 mg, 350 mmol).

Di-*tert*-butyl 2,2'-(((5-chlorothiophen-2-yl)methyl)azanediyl)diacetate (22h). Yellow solid, yield: 80% (510 mg, 1.36 mmol).

2,2'-(((5-Chlorothiophen-2-yl)methyl)azanediyl)diacetic acid (23h). Deprotection Procedure A. Dark yellow solid, yield: 98% (107 mg, 0.41 mmol).

Inhibition screening and IC$_{50}$ determination

A soluble truncation of NDM-1 was over-expressed and purified as described previously.[35] IC$_{50}$ values were determined using 11 concentrations of compound that span the IC$_{50}$ value, and were assayed using meropenem as described previously[25] except that total assay volumes were increased to 200 μL. Final DMSO concentrations (derived from compound stock solutions) were 1% (v/v). For initial screening of compounds, the percent inhibition at 200 μM and 250 μM for each compound was determined using a similar procedure. The NDM-1 catalyzed hydrolysis rate in the absence of added inhibitor (adjusted for constant DMSO concentration) was set at 100% activity (0% inhibition), and the relative rates determined in the presence of inhibitors were used to calculate percent inhibition with respect to that control (e.g. 90% activity is reported as 10% inhibition). Briefly, each compound (357 μM) was incubated with NDM-1 (3.6 nM) for 20 min at 25 °C and diluted upon addition of the meropenem substrate to initiate the reaction. Final concentrations: NDM-1 (2.5 nM), compound (200 μM and 250 μM), meropenem (180 μM), CHAPS (2 mM), HEPES (50 mM), DMSO (0.5 %) at pH 7. Assays were completed as described for the IC$_{50}$ determinations above.

Thermal Shift Assay

To each well of a 96-well 0.2 mL optical MicroAmp (ThermoFisher) thermocycler plate was added 9.5 μL of buffer (50 mM HEPES pH 7.5), 4 μL of NDM-1 in buffer (25 μM), 4 μL of

inhibitor in buffer (1 mM), and 2.5 μL of SYPRO orange Thermal Shift dye (ThermoFisher) in buffer. Each well contained a final concentration of 5 μM NDM-1 and 200 μM inhibitor. Thermocycler plate wells were sealed prior to analysis, and the plate was then heated in a thermocycler from 25 to 99 °C at a ramp rate of 0.05 °C/sec. Each thermal shift measurement was taken in eight replicates. Fluorescence was read using the ROX filter channel (λ_x = 580 nm; λ_{em} = 623 nm), and the T_M was determined by plotting the first derivative of the fluorescence emission as a function of temperature (-dF/dT) to identify T_M via Applied Biosystems® Protein Thermal Shift™ Software. Native NDM-1was observed to melt with a T_M = 55.95±0.06 °C.

Native state electrospray ionization mass spectrometry

NanoESI-MS was used to analyze the mechanism of inhibition of some of the inhibitors in this study. Expression and purification of NDM-1 and VIM-2 were performed according to literature reported procedures.[12a, 36] Samples (50 μM of VIM-2 and NDM-1) were incubated for 1 h and dialyzed overnight against 100 mM ammonium acetate, pH 7.5, after addition of tris(2-carboxyethyl) phosphine hydrochloride (TCEP, final concentration 2 mM) and 3 equivalents (VIM-2) or 2 equivalents (NDM-1) of Zn(II) (from a 0.1 M ZnCl2 stock). To analyze samples, a nano-electrospray ionization (n-ESI) probe (ThermoFisher Scientific, San Jose, CA, USA) with positive mode protein detection was used on a Thermo Scientific LTQ Orbitrap XL™ hybrid ion trap-orbitrap mass spectrometer. The major parameters were set as follows: capillary temperature, 180 °C; sheath gas, 0; auxiliary gas, 0; sweep gas, 0; spray voltage, 1.1-1.9kV; tube-lens, 150 V; capillary voltage, 35 V; full scan ranging 1000-4000 (m/z); and resolution set to 30,000. The automated gain control was set as follows: full scan, 3×10^4; SIM, 1×10^4; and MS^n 1×10^5 for Fourier-transform. Making slight modifications, the nESI source was equipped with an offline unite (Catalog number ES260) which was constructed based on previously published material.[37] To construct the source, a platinum white (0.25 mm diameter) was inserted into the center of the offline unit. The glass capillaries (inner tip diameter 0.8 mm, outer tip diameter 1.5 mm) were produced in-house using a micropipette puller (model P-87 Flaming/Brown Micropipette Puller, Sutter Instrument Inc., USA), 5 μL of sample was loaded into the pulled glass capillary. The platinum wire was inserted into the capillary and the capillary position was adjusted approximately 3 mm from the MS inlet.

Supplementary Material

Refer to Web version on PubMed Central for supplementary material.

Acknowledgements

References

[1]. Centers for Disease Control and Prevetion 2019, p. 148.

[2]. a) Bonomo RA, Cold Spring Harbor Perspect. Med 2017, 7, a025239;b) Fisher JF, Meroueh SO, Mobashery S, Chem. Rev 2005, 105, 395–424; [PubMed: 15700950] c) Munita JM, Arias CA, Microbiol. Spectr 2016, 4, VMBF-0016–2015.

[3]. Bush K, Bradford PA, Cold Spring Harb Perspect. Med 2016, 6.

[4]. Bush K, Jacoby GA, Antimicrob. Agents Chemother 2010, 54, 969–976. [PubMed: 19995920]

[5]. Sabath LD, Abraham EP, Biochem. J 1966, 98, 11–13.

[6]. a) Meini MR, Llarrull LI, Vila AJ, FEBS Lett. 2015, 589, 3419–3432; [PubMed: 26297824] b) Mojica MF, Bonomo RA, Fast W, Curr. Drug Targets 2016, 17, 1029–1050. [PubMed: 26424398]

[7]. a) Ju L-C, Cheng Z, Fast W, Bonomo RA, Crowder MW, Trends Pharmacol. Sci 2018, 39, 635–647; [PubMed: 29680579] b) Bush K, Bradford PA, Nat. Rev. Microbio 2019, 17, 295–306;c) Tooke CL, Hinchliffe P, Bragginton EC, Colenso CK, Hirvonen VHA, Takebayashi Y, Spencer J, J. Mol. Biol 2019, 431, 3472–3500. [PubMed: 30959050]

[8]. a) Drawz SM, Bonomo RA, Clin. Microbiol. Rev 2010, 23, 160–201; [PubMed: 20065329] b) Crowder MW, Spencer J, Vila AJ, Acc. Chem. Res 2006, 39, 721–728; [PubMed: 17042472] c) Nordmann P, Naas T, Poirel L, Emerging Infect. Dis 2011, 17, 1791–1798. [PubMed: 22000347]

[9]. Yong D, Toleman MA, Giske CG, Cho HS, Sundman K, Lee K, Walsh TR, Antimicrob. Agents Chemother 2009, 53, 5046–5054. [PubMed: 19770275]

[10]. Zou D, Huang Y, Liu W, Yang Z, Dong D, Huang S, He X, Ao D, Liu N, Wang S, Wang Y, Tong Y, Yuan J, Huang L, Sci. Rep 2017, 7, 9405. [PubMed: 28839253]

[11]. a) Gonzalez LJ, Bahr G, Nakashige TG, Nolan EM, Bonomo RA, Vila AJ, Nat. Chem. Biol 2016, 12, 516–522; [PubMed: 27182662] b) King D, Strynadka N, Protein Sci. 2011, 20, 1484–1491; [PubMed: 21774017] c) Bahr G, Vitor-Horen L, Bethel CR, Bonomo RA, Gonzalez LJ, Vila AJ, Antimicrob. Agents Chemother 2018, 62, e01849–01817. [PubMed: 29038264]

[12]. a) Cheng Z, Thomas PW, Ju L, Bergstrom A, Mason K, Clayton D, Miller C, Bethel CR, VanPelt J, Tierney DL, Page RC, Bonomo RA, Fast W, Crowder MW, J. Biol. Chem 2018, 293, 12606–12618; [PubMed: 29909397] b) Stewart AC, Bethel CR, VanPelt J, Bergstrom A, Cheng Z, Miller CG, Williams C, Poth R, Morris M, Lahey O, Nix JC, Tierney DL, Page RC, Crowder MW, Bonomo RA, Fast W, Acs Infect. Dis 2017, 3, 927–940; [PubMed: 28965402] c) Naas T, Oueslati S, Bonnin RA, Dabos ML, Zavala A, Dortet L, Retailleau P, Iorga BI, J. Enzyme Inhib. Med. Chem 2017, 32, 917–919. [PubMed: 28719998]

[13]. Kang JS, Zhang AL, Faheem M, Zhang CJ, Ai N, Buynak JD, Welsh WJ, Oelschlaeger P, J. Chem. Inf. Model 2018, 58, 1902–1914. [PubMed: 30107123]

[14]. Kim Y, Tesar C, Mire J, Jedrzejczak R, Binkowski A, Babnigg G, Sacchettini J, Joachimiak A, PLoS One 2011, 6, e24621. [PubMed: 21931780]

[15]. a) Sun Z, Hu L, Sankaran B, Prasad BVV, Palzkill T, Nat. Commun 2018, 9, 4524; [PubMed: 30375382] b) Zhang H, Hao Q, FASEB J. 2011, 25, 2574–2582. [PubMed: 21507902]

[16]. Linciano P, Cendron L, Gianquinto E, Spyrakis F, Tondi D, ACS Infect. Dis 2018, 5, 9–34. [PubMed: 30421910]

[17]. a) Li N, Xu Y, Xia Q, Bai C, Wang T, Wang L, He D, Xie N, Li L, Wang J, Zhou HG, Xu F, Yang C, Zhang Q, Yin Z, Guo Y, Chen Y, Bioorg. Med. Chem. Lett 2014, 24, 386–389; [PubMed: 24269122] b) King DT, Worrall LJ, Gruninger R, Strynadka NC, J. Am. Chem. Soc 2012, 134, 11362–11365; [PubMed: 22713171] c) Guo Y, Wang J, Niu G, Shui W, Sun Y, Zhou H, Zhang Y, Yang C, Lou Z, Rao Z, Protein Cell 2011, 2, 384–394; [PubMed: 21637961] d) Cain R, Brem J, Zollman D, McDonough MA, Johnson RM, Spencer J, Makena A, Abboud MI, Cahill S, Lee SY, McHugh PJ, Schofield CJ, Fishwick CWG, J. Med. Chem 2018, 61, 1255–1260. [PubMed: 29271657]

[18]. a) Cahill ST, Cain R, Wang DY, Lohans CT, Wareham DW, Oswin HP, Mohammed J, Spencer J, Fishwick CW, McDonough MA, Schofield CJ, Brem J, Antimicrob. Agents Chemother 2017, 61;b) Brem J, Cain R, Cahill S, McDonough MA, Clifton IJ, Jimenez-Castellanos JC, Avison MB, Spencer J, Fishwick CW, Schofield CJ, Nat. Commun 2016, 7, 12406; [PubMed: 27499424] c) Krajnc A, Brem J, Hinchliffe P, Calvopina K, Panduwawala T, Lang PA, Kamps J, Tyrell JM,

Widlake E, Saward BG, Walsh TR, Spencer J, Schofield CJ, J. Med. Chem 2019, 62, 8544–8556. [PubMed: 31454231]

[19]. a) Zhang E, Wang MM, Huang SC, Xu SM, Cui DY, Bo YL, Bai PY, Hua YG, Xiao CL, Qin S, Bioorg. Med. Chem. Lett 2018, 28, 214–221; [PubMed: 29248295] b) Schnaars C, Kildahl-Andersen G, Prandina A, Popal R, Radix S, Le Borgne M, Gjoen T, Andresen AMS, Heikal A, Okstad OA, Frohlich C, Samuelsen O, Lauksund S, Jordheim LP, Rongved P, Astrand OAH, ACS Infect. Dis 2018, 4, 1407–1422; [PubMed: 30022668] c) Yu ZJ, Liu S, Zhou S, Li H, Yang F, Yang LL, Wu Y, Guo L, Li GB, Bioorg. Med. Chem. Lett 2018, 28, 1037–1042; [PubMed: 29477271] d) Chen AY, Thomas PW, Stewart AC, Bergstrom A, Cheng ZS, Miller C, Bethel CR, Marshal SH, Credille CV, Riley CL, Page RC, Bonomo RA, Crowder MW, Tierney DL, Fast W, Cohen SM, J. Med. Chem 2017, 60, 7267–7283; [PubMed: 28809565] e) King AM, Reid-Yu SA, Wang W, King DT, De Pascale G, Strynadka NC, Walsh TR, Coombes BK, Wright GD, Nature 2014, 510, 503–506; [PubMed: 24965651] f) Liu S, Zhou Y, Niu X, Wang T, Li J, Liu Z, Wang J, Tang S, Wang Y, Deng X, Cell Death Discovery 2018, 4, 28.

[20]. a) Bergstrom A, Katko A, Adkins Z, Hill J, Cheng Z, Burnett M, Yang H, Aitha M, Mehaffey MR, Brodbelt JS, Tehrani K, Martin NI, Bonomo RA, Page RC, Tierney DL, Fast W, Wright GD, Crowder MW, ACS Infect. Dis 2018, 4, 135–145; [PubMed: 29091730] b) Zhang J, Wang S, Wei Q, Guo Q, Bai Y, Yang S, Song F, Zhang L, Lei X, Bioorg. Med. Chem 2017, 25, 5133–5141. [PubMed: 28784300]

[21]. a) Albu SA, Koteva K, King AM, Al-Karmi S, Wright GD, Capretta A, Angew. Chem., Int. Ed. Engl 2016, 55, 13259–13262; [PubMed: 27633338] b) Tehrani K, Fu H, Bruchle NC, Mashayekhi V, Prats Lujan A, van Haren MJ, Poelarends GJ, Martin NI, Chem. Commun 2020, [Online early access], DOI: 10.1039/D1030CC00356E;c) Proschak A, Kramer J, Proschak E, Wichelhaus TA, J. Antimicrob. Chemother 2018, 73, 425–430. [PubMed: 29186432]

[22]. a) Liao D, Yang S, Wang J, Zhang J, Hong B, Wu F, Lei X, Angew. Chem., Int. Ed. Engl 2016, 55, 4291–4295; [PubMed: 26592805] b) Koteva K, King AM, Capretta A, Wright GD, Angew. Chem., Int. Ed. Engl 2016, 55, 2210–2212; [PubMed: 26709849] c) Zhang J, Wang S, Bai Y, Guo Q, Zhou J, Lei X, J. Org. Chem 2017, 82, 13643–13648. [PubMed: 29115130]

[23]. Ni LB, Zhang RH, Liu QX, Xia WS, Wang H, Zhou ZH, Solid State Chem J. 2009, 182, 2698–2706.

[24]. Raczynska JE, Shabalin IG, Minor W, Wlodawer A, Jaskolski M, Drug Resist. Updat 2018, 40, 1–12. [PubMed: 30466711]

[25]. Chen AY, Thomas PW, Cheng Z, Xu NY, Tierney DL, Crowder MW, Fast W, Cohen SM, ChemMedChem 2019, 14, 1271–1282. [PubMed: 31124602]

[26]. Krezel A, Maret W, Arch. Biochem. Biophys 2016, 611, 3–19. [PubMed: 27117234]

[27]. Cheng Y, Prusoff WH, Biochem. Pharmacol 1973, 22, 3099–3108. [PubMed: 4202581]

[28]. Pantoliano MW, Petrella EC, Kwasnoski JD, Lobanov VS, Myslik J, Graf E, Carver T, Asel E, Springer BA, Lane P, Salemme FR, J. Biomol. Screen 2001, 6, 429–440. [PubMed: 11788061]

[29]. Klingler FM, Wichelhaus TA, Frank D, Cuesta-Bernal J, El-Delik J, Muller HF, Sjuts H, Gottig S, Koenigs A, Pos KM, Pogoryelov D, Proschak E, J. Med. Chem 2015, 58, 3626–3630. [PubMed: 25815530]

[30]. Credille CV, Morrison CN, Stokes RW, Dick BL, Feng Y, Sun J, Chen Y, Cohen SM, J. Med. Chem 2019, 62, 9438–9449. [PubMed: 31536340]

[31]. Lo MC, Aulabaugh A, Jin G, Cowling R, Bard J, Malamas M, Ellestad G, Anal. Biochem 2004, 332, 153–159. [PubMed: 15301960]

[32]. a) Selevsek N, Tholey A, Heinzle E, Lienard BMR, Oldham NJ, Schofield CJ, Heinz U, Adolph H-W, Frere J-M, J. Am. Soc. Mass Spectrom 2006, 17, 1000–1004;b) Heck AJR, Nat. Methods 2008, 5, 927–933. [PubMed: 18974734]

[33]. Stokvis E, Rosing H, Beijnen JH, Rapid Commun. Mass Spectrom 2005, 19, 401–407. [PubMed: 15645520]

[34]. a) Paramella D, Cantel S, Enjalbal C, Amblard M, Forest E, Heymann M, Geourjon C, Martinez J, Subra G, Proteomics 2009, 9, 5384–5388; [PubMed: 19902427] b) Rolland O, Turrin C-O, Baquet G, Poupot R, Poupot M, Caminade A-M, Majoral J-P, Tet. Lett 2009, 50, 2078–2082.

[35]. Yang H, Aitha M, Hetrick AM, Richmond TK, Tierney DL, Crowder MW, Biochemistry 2012, 51, 3839–3847. [PubMed: 22482529]

[36]. Cheng Z, Shurina BA, Bethel CR, Thomas PW, Marshall SH, Thomas CA, Yang K, Kimble RL, Montgomery JS, Orischak MG, Miller CM, Tennenbaum JL, Nix JC, Tierney DL, Fast W, Bonomo RA, Page RC, Crowder MW, mBio 2019, 10, e02412–02419. [PubMed: 31744917]

[37]. Harvey SR, Porrini M, Stachl C, MacMillan D, Zinzalla G, Barran PE, J. Am. Chem. Soc 2012, 134, 19384–19392. [PubMed: 23106332]
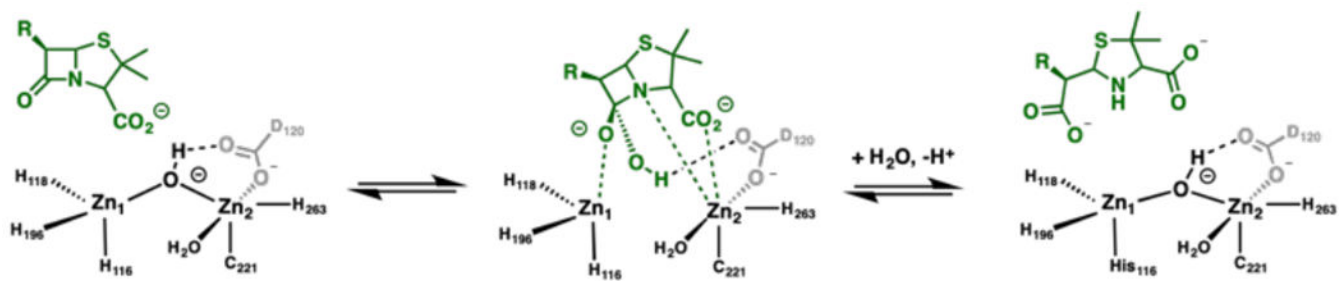
Figure 1.
Scheme of the NDM active site and a proposed hydrolysis mechanism of the β-lactam antibiotic penicillin.
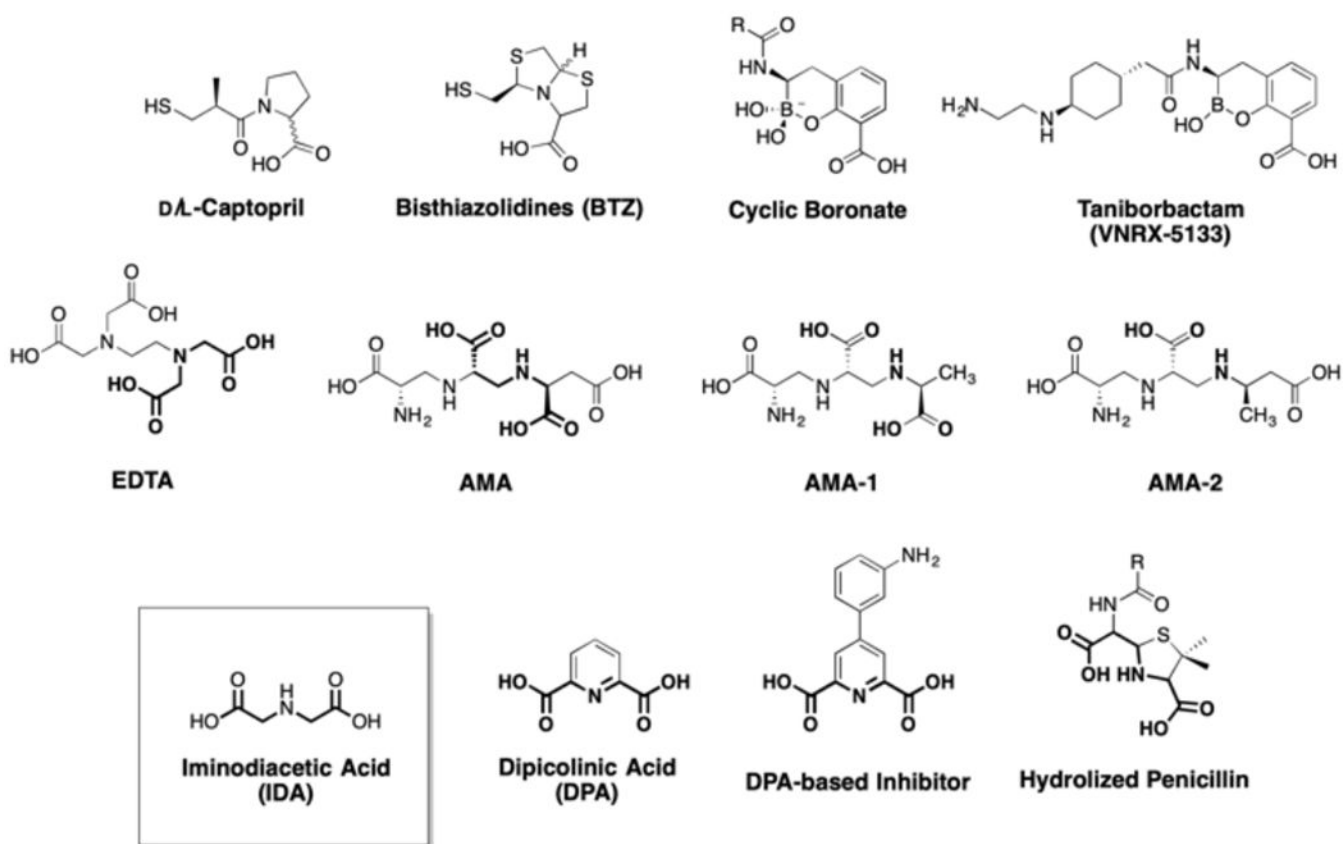
Figure 2.
Representative inhibitors of NDM-1.
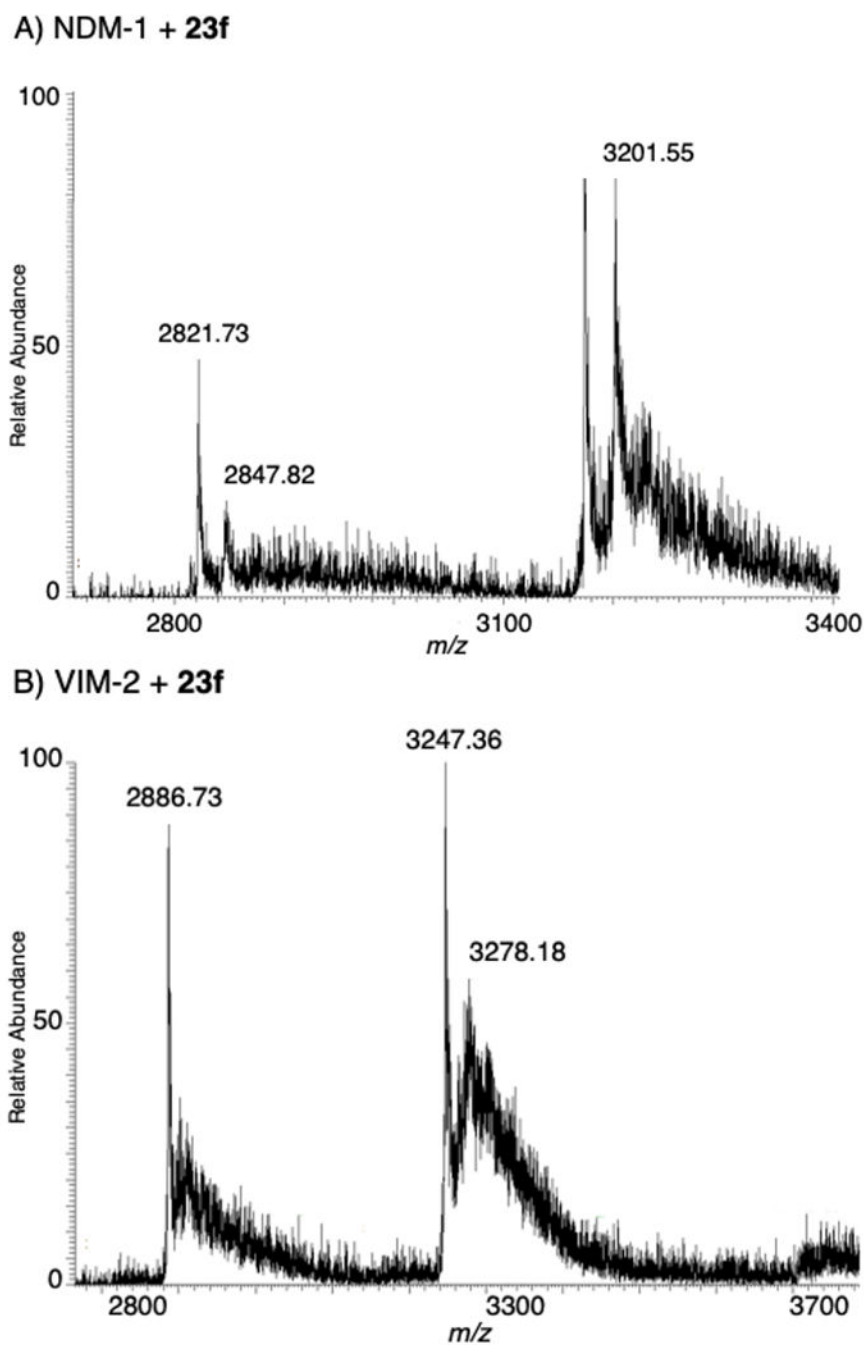
Figure 3.
Native state ESI-MS of lead inhibitor **23f** with: NDM-1 *(top)* and VIM-2 *(bottom)*.
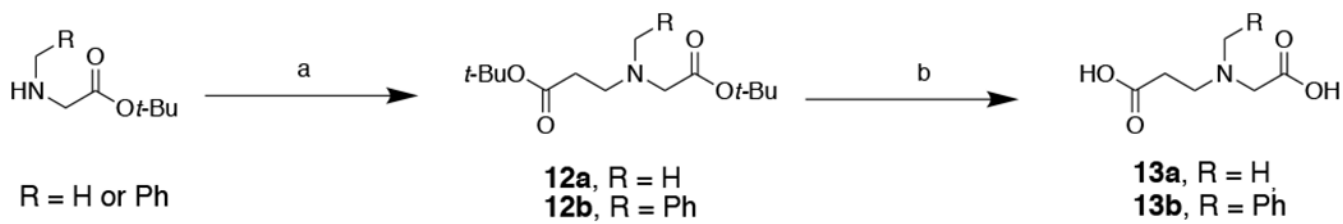
Scheme 1.
Synthesis of **13a** and **13b**. Reagents and conditions: (a) *t*-butyl acrylate, TEA, EtOH, 65 °C, 16 h, 43 – 90%; (b) TFA:CH$_2$Cl$_2$, 25 °C, 16 h, ~99%.
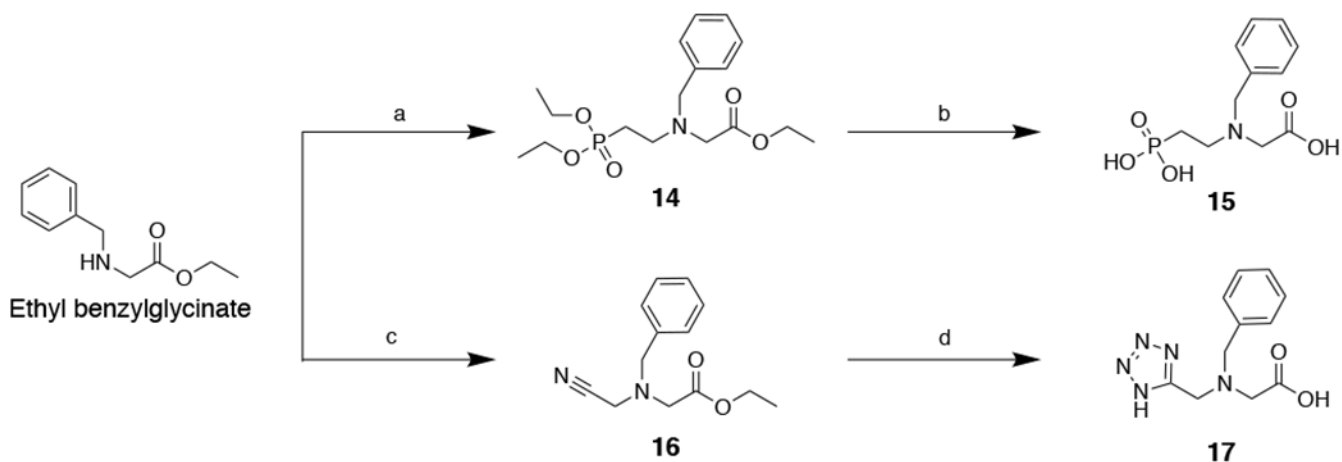
Scheme 2.
Synthesis of **IDA** inhibitors **15** and **17**. Reagents and conditions: (a) diethyl(2-bromoethyl)phosphonate, K_2CO_3, KI, ACN, 82 °C, 16 h, 40%; (b) HCl, 100 °C, 16 h, ~99%; (c) 2-bromoacetonitrile, K_2CO_3, KI, CH_3CN, 25 °C, 16 h, 74%; (d) NaN_3, NH_4Cl, DMF, 110 °C, 16 h; then 1:1:1 MeOH:THF:1 M NaOH, 60 °C, 16 h; two steps 19%.
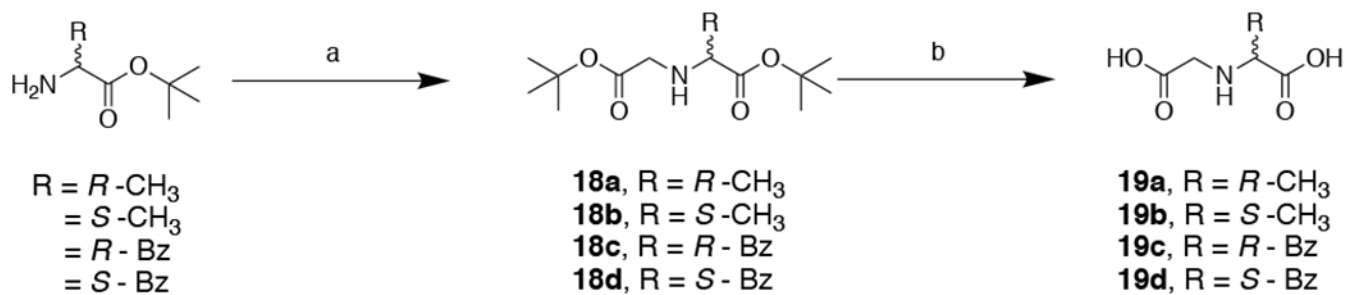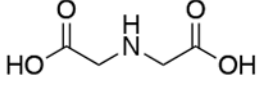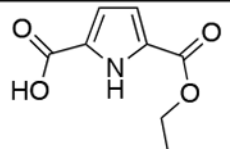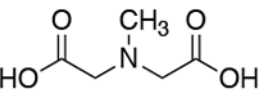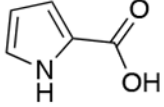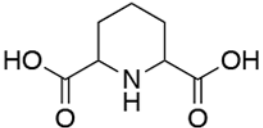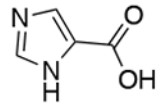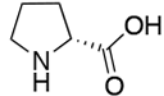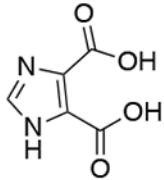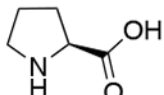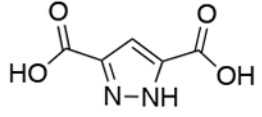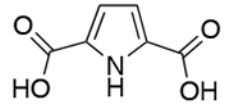
Scheme 3.
Synthesis of **19a** – **19d**. Reagents and conditions: (a) *t*-butyl 2-bromoacetate, TEA, DMF, 0 – 25 °C, 16 h, 40 – 54%; (b) TFA, CH_2Cl_2, 25 °C, 16 h, ~99%.
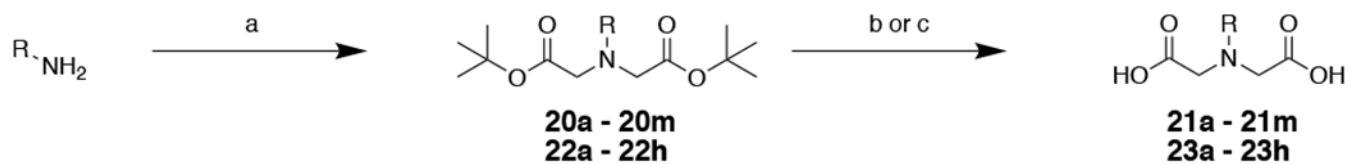
Scheme 4.
Synthesis of **IDA** inhibitors **21a** – **21m** and **23a** – **23h**. Reagents and conditions: (a) *t*-butyl 2-bromoacetate, KHCO$_3$, THF, 25 °C, 16 h, 25 – 98%; (b) TFA, CH$_2$Cl$_2$, 25 °C, 16 h or (c) MeOH:THF:1M NaOH, 100 °C, 16 h, 29 – 99%.
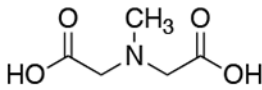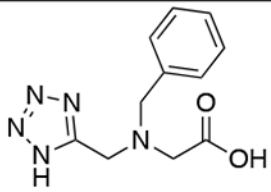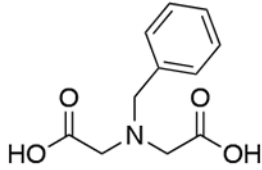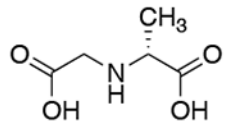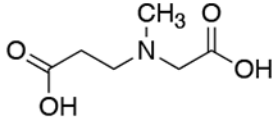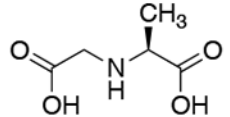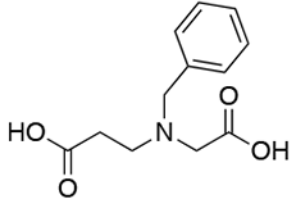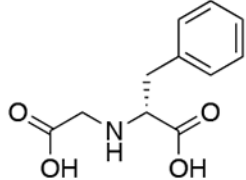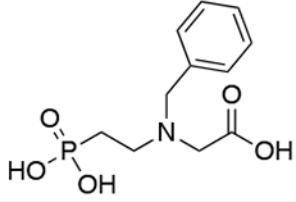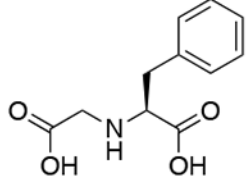
Table 1.

Percent Inhibition of **IDA** derived MBPs (at 200 μM) against NDM-1.[a]

Compound		% Inhibition	Compound		% Inhibition
IDA		48±2	**6**		3±10
1		80±4	**7**		0
2		8±7	**8**		57±4
3		0	**9**		28±1
4		0	**10**		33±5
5		4±4			

[a] Values are the average of triplicates experiments with standard deviations shown.
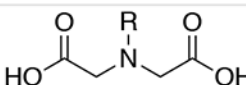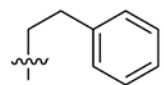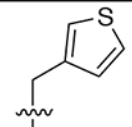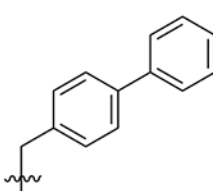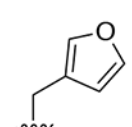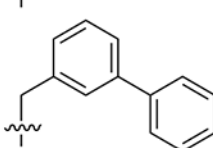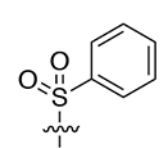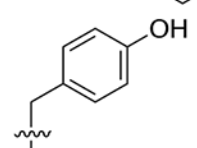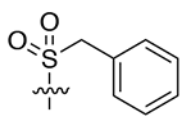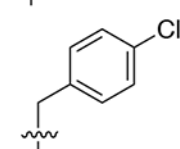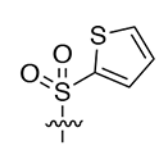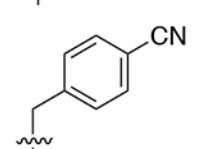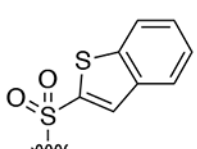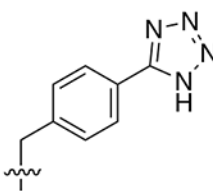
Table 2.
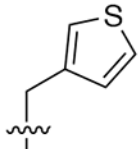
Percent Inhibition of **IDA** derivatives (at 250 μM) against NDM-1.[a]

Compound		% Inhibition	Compound		% Inhibition
1		90±1	**17**		43±1
11		65±1	**19a**		53±2
13a		0	**19b**		51±1
13b		0	**19c**		54±1
15		0	**19d**		65±1

[a]Values are the average of triplicates experiments with standard deviations shown.
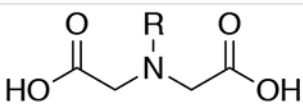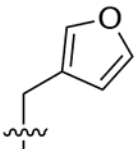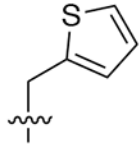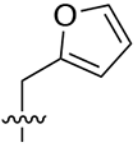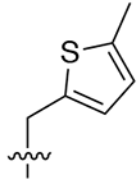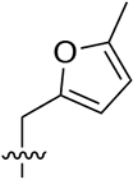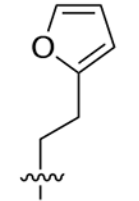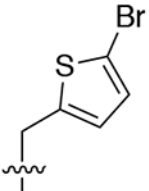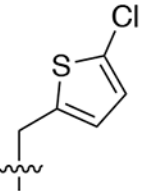
Table 3.

Inhibitory activity of **21a** – **21m** (at 250 μM) against NDM-1.[a]

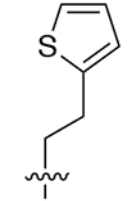| Compound		% Inhibition	Compound		% Inhibition
21a		70±1	**21h**		64±2
21b		56±2	**21i**		99±7
21c		76±6	**21j**		0
21d		66±2	**21k**		0
21e		36±2	**21l**		20±5
21f		74±2	**21m**		21±8
21g		67±2			

[a]Values are the average of triplicates experiments with standard deviations shown.

Table 4.

Inhibitory activity of **IDA** derivatives **23a** – **23h** against NDM-1.[a]

Compound		IC$_{50}$ (µM)	Compound		IC$_{50}$ (µM)
IDA	H	120±10	**1**	CH$_3$	25±2
21h		172±8	**21i**		32±3
23a		66±3	**23b**		22±1
23c		91±8	**23d**		47±4
23e		51±2	**23f**		8.6±0.2
23g	Br	32±2	**23h**	Cl	46±2

[a]Values are the average of triplicate experiments with fitting errors shown.

Table 5.

Protein thermal shift of selected compounds against NDM-1. [a]

Compound	T_m (°C)	Compound	T_m (°C)
L-Captopril	4.61±0.07	**DPA**	−14.5±0.2
IDA	4.39±0.04	**1**	1.9±0.2
21h	4.43±0.07	**21i**	3.4±0.3
23a	3.1±0.1	**23b**	1.6±0.4
23c	5.2±0.1	**23d**	3.4±0.2
23e	1.7±0.2	**23f**	1.5±0.1
23g	3.0±0.3	**23h**	4.2±0.2

[a]Values are the average of eight replicates with standard deviations shown. Native NDM-1 was observed to melt at T_M = 55.95±0.06 °C.

Table 6.

Summary of the native ESI-MS experimental results for NDM-1.[a]

Sample	NDM-1 + Inhibitor Complex Mass (Da)	Peak Charge (+)	Predicted Peak (m/z)	Observed Peak (m/z)	Complex
NDM-1	25,385	9	2,821	2,822	2Zn: NDM-1
	25,385	10	2,539	2,540	2Zn: NDM-1
NDM-1 + **DPA**	25,255	9	2,807	2,807	0Zn: NDM-1
	25,320	9	2,814	2,814	1Zn: NDM-1
	25,385	9	2,821	2,821	2Zn: NDM-1
NDM-1 + **1**	25,532	9	2,838	2,837	2Zn: NDM-1:**1**
NDM-1 + **23c**	25,628	9	2,848	2,850	2Zn: NDM-1:**23c**
		8	3,204	3,210	2Zn: NDM-1:**23c**
NDM-1 + **23d**	25,612	9	2,847	2,846	2Zn: NDM-1:**23d**
		8	3,202	3,202	2Zn: NDM-1:**23d**
NDM-1 + **23e**	25,628	9	2,848	2,847	2Zn: NDM-1:**23e**
		8	3,204	3,205	2Zn: NDM-1:**23e**
NDM-1 + **23f**	25,612	9	2,847	2,848	2Zn: NDM-1:**23f**
		8	3,202	3,202	2Zn: NDM-1:**23f**

[a] Percent error was calculated by subtracting the expected peak value from the actual peak value, dividing by the expected peak value and multiplying by 100 and all observed to be <0.2%.

Table 7.

Summary of the native ESI-MS experimental results for VIM-2.[a]

Sample	NDM-1 + Inhibitor Complex Mass (Da)	Peak Charge (+)	Predicted Peak (*m/z*)	Observe d Peak (*m/z*)	Complex
VIM-2	25,972	9	2,887	2,886	2Zn: VIM-2
	25,972	8	3,247	3,247	2Zn: VIM-2
VIM-2 + **DPA**	26,010	9	2,891	2,891	0Zn: VIM-2:**DPA**
	26,010	8	3,252	3,253	0Zn: VIM-2:**DPA**
VIM-2 + **1**	26,119	9	2,903	2,902	2Zn: VIM-2:**1**
VIM-2 + **23c**	26,215	8	3,278	3,277	2Zn: VIM-2:**23c**
VIM-2 + **23d**	26,199	8	3,276	3,276	2Zn: VIM-2:**23d**
VIM-2 + **23e**	26,215	8	3,278	3,277	2Zn: VIM-2:**23e**
VIM-2 + **23f**	26,199	8	3,276	3,278	2Zn: VIM-2:**23f**

[a]Percent error was calculated by subtracting the expected peak value from the actual peak value, dividing by the expected peak value and multiplying by 100 and all observed to be <0.07%.